Suggested Citation

M. Gulzar, H.H. Masjuki, M. Varman, M.A. Kalam, R.A Mufti, NWM Zulkifli, R. Yunus and Rehan Zahid " Improving the AW/EP ability of chemically modified palm oil by adding CuO and MoS_2 nanoparticles" Tribology International 88 (2015): 271–279.

Improving the AW/EP Ability of Chemically Modified Palm Oil by Adding CuO and MoS_2 Nanoparticles

M.Gulzar[1*], HH Masjuki[2], M Varman[3**], MA Kalam[4], R.A. Mufti[5], NWM Zulkifli[6], R. Yunus[7], Rehan Zahid[8]

[1,2,3,4,6,8] Centre for Energy Sciences, Department of Mechanical Engineering, University of Malaya, Kuala Lumpur-50603, MALAYSIA

[5] NUST School of Mechanical and Manufacturing Engineering, National University of Sciences and Technology (NUST), H-12, Islamabad-44000, PAKISTAN

[7] Institute of Advanced Technology, University Putra Malaysia, Serdang, Selangor-43400, MALAYSIA

[1]Research Assistant <mubashir_nustian@hotmail.com>

[2]Professor<masjuki@um.edu.my>

[3]Senior Lecturer<mahendra@um.edu.my >

[4]Senior Lecturer<kalam@um.edu.my >

[5]Professor <riazmufti@smme.nust.edu.pk >

[6]Research Fellow<nurinmz@um.edu.my>

[7]Professor <robiah@eng.upm.edu.my>

[*]Corresponding author

Tel.: +60 3 79674448; fax: +60 3 79675317.

E-mail addresses: mubashir_nustian@hotmail.com; mahendra@um.edu.my,

Centre for Energy Sciences, Department of Mechanical Engineering,

University of Malaya, Kuala Lumpur-50603, MALAYSIA

Abstract

Improvement in the anti-wear (AW) and extreme pressure (EP) ability of chemically modified palm oil (CMPO) by adding nanoparticles was experimentally evaluated. Nanolubricants were synthesized by adding 1 wt% copper(II) oxide (CuO) and 1 wt% molybdenum disulfide (MoS_2) nanoparticles to CMPO. The AW/EP properties of the formulations were evaluated by four-ball and sliding wear tests. Wear surfaces were analyzed by scanning electron microscopy, along with energy-dispersive X-ray and micro-Raman scattering spectroscopy. The MoS_2 nanoparticles exhibited better AW/EP properties than did the CuO nanoparticles. The addition of 1 wt% oleic acid as a surfactant facilitated the reduction of agglomerates.

1. Introduction

The depletion of conventional energy sources and the need to reduce environmental emissions have urged researchers to investigate green or renewable energy alternatives. In this regard, oil from agricultural feedstocks is a suitable substitute for petroleum lubricants because vegetable based lubricants presents biodegradability, nontoxicity, and easy disposal. Despite the benefits derived from such lubricants, however, directly using vegetable oils as lubricants is unfavorable because they have low thermal and oxidation stability. These deficiencies have been improved via the inducement of chemical changes, such as esterification, epoxidation, and hydroxylation. Research has shown that chemically modified biolubricants that are extracted from vegetable oils exhibit excellent oxidation stability and low-temperature flow properties [1-3]. Nevertheless, the resistance to extreme pressure and anti-wear characteristics (hereafter referred to in this paper as “AW/EP properties/characteristics”) of these lubricants are questionable when evaluated against those of commercial petroleum oils with anti-wear

additives [4]. Zulkifli et al. revealed that palm oil trimethylolpropane (TMP) ester exhibits poorer anti-wear characteristics than that presented by ordinary commercial lubricants [3]. These drawbacks prompted researchers to use raw vegetable oils and chemically modified vegetable oils as additives to commercial lubricants [3, 5, 6]. The prospect of solving the aforementioned problems improved with the advent of nanotribology, whose development was facilitated by the introduction of nanotechnology in recent years. The lubrication-enhancing ability of nanoparticles is related to a variety of mechanisms, including the effects of ball bearings, polishing, mending, and protective film formation [7-13]. An important consideration in nanotribological techniques is that producing effective suspensions necessitates compatibility between selected nanoparticles and base oils [14]. In various research experiments, oxides and chalcogenides showed good compatibility with selected base oils and superior wear prevention characteristics; these materials include copper(II) oxide (CuO) [10, 14-19], zinc oxide (ZnO) [15, 17, 20], zirconium dioxide (ZrO_2) [15, 17, 21], titanium dioxide (TiO_2) [10, 22], silicon dioxide (SiO_2) [22], aluminium oxide (Al_2O_3) [23], as well as molybdenum disulfide (MoS_2) [24-28] and tungsten disulfide (WS_2) [29, 30]. In spite of the progress made in research, however, only a few tribological studies have been devoted to vegetable oil-based nanolubricants [14, 16, 19]. Introducing CuO nanoparticles in coconut oil and chemically modified rapeseed oil helps reduce sliding wear and friction [16, 19]. A rapeseed oil-based nanolubricant has also been tested on actual engine and has been found comparable to commercial counterparts [31]. In another experimental study, researchers found that adding CuO and ZnO to sunflower and soybean-based biolubricants cannot effectively enhance wear protection [14].

Using vegetable-based oil as an effective lubricant necessitates high load-carrying capacity and effective lubrication under a wide range of speeds, temperatures, and contact geometries. Recent advancements in nanotribology paved the way for improving the AW/EP properties of

mineral and synthetic base oils. To the best of our knowledge, no technical studies have explored nanoMoS_2 and nanoCuO as AW/EP additives for TMP ester produced from palm oil. To address this gap, the present study investigates the AW/EP characteristics of CMPO enriched with nanoMoS_2 and nanoCuO for conformal and non-conformal contact geometries at different test conditions. For this purpose, 1 wt% CuO and 1 wt% MoS_2 nanoparticles are used as AW/EP additives. Formulations with 1 wt% nanoparticles and 1 wt% oleic acid are also synthesized to analyze the effects of anionic surfactant on nanoparticle dispersion and tribological characteristics. This study is divided into two stages. The first involves four-ball testing, which is conducted to evaluate the AW/EP characteristics of the oil samples. The features of wear scars at different normal loadings are used to compare the AW/EP characteristics of the lubricant samples. In the second stage, the nanolubricants are tested for piston ring and cylinder liner interaction by using a high-stroke reciprocating test rig. After the series of tribological tests, worn surfaces are analyzed by scanning electron microscopy (SEM), energy-dispersive X-ray (EDX) spectroscopy, and micro-Raman spectroscopy to determine the improvement in the AW/EP properties of the nanolubricants.

2. Materials and methods

2.1. Preparation of CMPO

Polyol ester was synthesized for use as a biolubricant. In the synthesis, palm-based methyl esters (POME) were used as starting materials, and TMP was used as a polyol. CMPO is produced when the transesterification reaction replaces an ester group from POME (i.e., RCOO–) with an –OH group from TMP. Given that three –OH groups exist in TMP, the process results in an intermediate formation of monoesters, diesters, and triesters. Methanol, a

by-product, was removed to ensure that the reaction was completed. The overall reaction is illustrated in **Fig. 1.**

Fig.1. Overall reaction for synthesis of CMPO

2.1.1. Transesterification

Reaction was induced in a 500-mL three-necked flask equipped with a reflux condenser, a thermometer, and a sampling port. The condenser was coupled to a vacuum line with a relief valve, an accumulator, and a vacuum trap. The reactor was then immersed in a temperature-controlled silicon oil bath, and the solution was agitated with a magnetic stirrer. A 200-g volume of methyl ester and a known amount of TMP were placed in the reactor, and the mixture was heated to the operating temperature before a catalyst was added. Vacuum was gradually applied after catalyst addition to avoid the spillover of reaction materials. TMP triesters were obtained at a POME-to-TMP molar ratio of 10:1. This ratio helped maintain the reaction temperature by providing a heat reservoir and driving forward reaction. Sodium methoxide was used as the catalyst because it minimizes the saponification of esters. The amount of catalyst used was 0.4% w/w, determined on the basis of the total mass at a 10:1 molar ratio. Samples were taken at pre-determined time intervals for the gas chromatographic analysis of product yield.

2.1.2. Product purification

After the reaction was completed, the catalyst was separated from the product mixture by vacuum filtration. Vacuum distillation was conducted to remove un-reacted methyl esters from the final product.

2.2. Synthesis of nanolubricants

Initially both the CuO and MoS_2 nanoparticles were added separately at six wt % concentrations: 0.25 %, 0.5%, 0.75%, 1%, 1.25% and 1.5%. For both test geometries, the nanolubricants with 1 wt% concentrations exhibited better wear protection except for a few variations at high concentrations. Thus, these nanolubricants were synthesized by dispersing 1 wt% nanoCuO and 1 wt% nanoMoS_2 in CMPO. Commercially available nanoparticles were obtained from M/S Sigma-Aldrich (M) (Sdn. Bhd., Malaysia), and the true size and density of the nanoparticles were provided by the supplier. **Figs. 2(a)** and **2(b)** show the morphology of the nanostructures of the CuO and MoS_2 nanoparticles. The morphology of the CuO nanoparticles was fairly spherical, with particle sizes between 50 and 300 nm. The particles of the MoS_2 powder had larger sizes, ranging from 50 to 2000 nm. The data were statistically analyzed by measuring the size of isolated nanoparticles on the basis of several different SEM micrographs (500 particles). The size distribution and mean of the nanoparticles are provided in **Fig. 3**. **Table 1** presents the detailed materials properties of the nanoparticles used in this study. The CuO (1 wt%) and MoS_2 (1 wt%) nanoparticles were dispersed in CMPO by immersion in an ultrasonic bath for 2 h at 30 °C. Two trial lubricant samples were synthesized with oleic acid as a surfactant (S) to study the effects of the anionic surfactant on nanoparticle dispersion and tribological properties. The nanoparticles (1 wt%) were dispersed in oleic acid (1 wt%), after which the mixture was dispersed in CMPO by immersion in an ultrasonic bath for 2 h to obtain a stable suspension. The relevant physicochemical properties of all the lubricant samples are given in **Table 2**.

Fig.2. SEM micrographs of (a) CuO nanoparticles (b) MoS_2 nanoparticles.

Fig.3. Lognormal size distribution with mean particle size (a) nanoCuO (b) nanoMoS2

Table 1. Material properties of nanoparticles

Table 2. Physicochemical properties of lubricant samples

2.3 Dispersibility of nanoparticles in CMPO

The dispersibility of the nanolubricant samples was evaluated by measuring the corresponding optical absorbance spectrum. A SPEKOL 1500 UV VIS Spectrophotometer with a wavelength of 429 nm and a repeatability of 1 nm was used. The nanolubricant samples were placed in glass cuvettes, and CMPO was used as a reference solution. The rate at which changes in the absorbance of visible light occurred was observed to evaluate the dispersive ability of the nanoparticles and the effectiveness of the surfactant. **Fig. 4** indicates that the lubricant samples dispersed with the MoS_2 nanoparticles were more stable than the nanoCuO-enriched lubricants. The dispersibility of the CuO nanoparticles was significantly enhanced by the addition of the surfactant, whereas that of the MoS_2 nanoparticles was minimally affected. The nanolubricants enriched with the MoS_2 nanoparticles produced homogeneous dispersion, whereas the CuO-enriched suspensions tended to isolate into sediments at the end of the dispersion analysis.

Fig. 4. The optical absorbance spectrum of nanolubricant samples over time.

2.4. Four-ball tests

A four-ball test configuration was used to investigate AW/EP characteristics under Hertzian contact loading. In this series of experiments, CMPO was treated as the reference oil to analyze the behavior of the nanosuspensions. The balls used were AISI 52100 steel balls with a diameter of 12.7 mm and an HRC hardness of 64–66. The balls and the pot were thoroughly cleaned with toluene before each experiment. The AW/EP test was performed in accordance with the ASTM D2783 standard. The significant experimental conditions are summarized in **Table 3**. Commonly used wear parameters, namely, the load–wear index (LWI), last non-seizure load (LNSL), initial seizure load (ISL), and weld point (WP), were evaluated. The results for these parameters were employed in analyzing wear protection, value of transition loading from the elastohydrodynamic regime to boundary lubrication, and point of seizure [32]. Accordingly, an initial 40-kg load was applied for the EP test and the normal loading was gradually increased until the balls were welded. The diameters of the wear scars on the balls were measured at all the loadings, thereby enabling the investigation of wear for all the lubricant samples. **Table 4** presents the average values of the maximum, minimum, and mean wear scar diameters, as well as the standard deviations (SDs). The related procedures and repeatability of results were verified on the basis of ASTM D2783 recommendations. The schematic plot of the scar diameters against the applied loads shows the LNSL and ISL at different loadings **(Fig. 5)**.

Table 3. Test conditions for four-ball tests.

Table 4. Wear scar diameter of test balls.

Fig. 5. Load vs. wear scar diameter (WSD) of CMPO+ nanoparticles suspensions.

2.5. Piston ring on the cylinder liner tests

To simulate actual engine conditions, specimens were extracted from the top compression piston ring and the cylinder liner of a commercial single-cylinder agricultural diesel engine. A CNC wire-cut EDM was used to machine the samples to prevent damage to surface finish and treatments. A high-stroke reciprocating test rig was used to ensure that the piston ring was stationary in the ring holder at the top and that the specimen of the cylinder liner exhibited a reciprocating motion. The specimen taken from the cylinder liner was placed in a lubricant bath, where the oil temperature was regulated using a control panel. After load application, the piston ring established conformal contact with the surface of the cylinder liner. Normal load was distributed in a uniform manner across the contact area. To simulate engine oil temperature, the oil bath was equipped with a temperature controller, a thermocouple, and a heater system. In this stage, the wear properties of the piston ring and cylinder liner were measured under the testing conditions indicated in **Table 5**. The considered loading conditions were used to simulate a maximum engine speed of 1.1 m/s and a contact pressure of ∼10 MPa, following the test conditions stated by Gullac and Akalin [29]. The experimental arrangement is illustrated in **Fig. 6**. Wear was measured using the weight loss method. The samples were ultrasonically cleaned and weighed to an accuracy of 0.1 mg before and after each test. Each test in the series was conducted with a new ring and cylinder liner specimen. Running in duration lasted for 2 h; thus, rough edges on new surfaces were shaved off before each test.

Table 5. Test parameters with values for ring on cylinder liner test.

2.6. Worn surface analysis

The characteristics of the wear scar surfaces were analyzed using a Hitachi SU8000 scanning electron microscope, and an electron-accelerating voltage of 5 kV was adopted. EDX spectroscopy (Oxford Instruments) was conducted to identify the elements existing on the selected wear scar surfaces. The Raman spectra of the possible tribofilms formed on the tested surfaces of the cylinder liner specimens were recorded using an InVia Raman microscope with an argon-ion laser having an excitation wavelength of 514 nm and a laser power of 10 mW.

Fig. 6. Experimental setup for piston ring on cylinder liner wear testing.

3. Results and discussion

3.1. AW and EP performance analyses

The comparison of the data in **Table 4** shows that the wear scar diameters were reduced by CMPO+1%MoS_2 (Oil D) and CMPO+1% MoS_2+1%S (Oil F) under all the loading conditions. The average decreases in wear scar diameters were 4.95% and 6.65% for oils D and F, respectively. The analysis of the curves in **Fig. 5** indicates that the LNSL increased from 70 to 80 kg for both oils D and F. The curves of the MoS_2 particle-enriched oils shifted to the lower side compared with the position of the CMPO curve when the cantilever load was increased to 80 kg or higher. This result reflects the effectiveness of MoS_2 nanoparticles under extreme loading conditions. An increase of about 1% in the average wear scar diameter was

observed in the oil samples enriched with CuO particles; such increase is attributed to the high wear scar diameters that these particles produced at low loads. The CuO particles exhibited superior resistance to extreme pressure at cantilever loads of 80 kg or higher. The wear scar diameter visibly decreased to 7.7% and 11% at 120-kg loading for CMPO+1%CuO (Oil C) and CMPO+1%CuO+1%S (Oil E), respectively **(Table 4)**. The addition of the surfactant improved the wear behavior of the blank oil as an average reduction of 2% occurred with the use of CMPO+1%S (Oil B). All the nanoparticle-enriched oils exhibited superior wear characteristics at high loads. An average reduction of 16.6% at loads higher than 80 kg was achieved with the wear scar diameters. This reduction is higher than that achieved (10%) in a lower load range. The MoS_2 and CuO nanoparticles tended to present excellent resistance to extreme pressure. Moreover, the MoS_2-enriched lubricants outperformed the other trial oils at low and high loads. **Table 6** shows the data on the resultant wear parameters of all the trial oils. The LWI values indicate that CMPO dispersed with the MoS_2 nanoparticles exhibited excellent wear protection. Similarly, considerably high values of all the other wear protection parameters were obtained with the MoS_2-enriched lubricants. Interestingly, the LWI of CMPO+1%S was low, indicating that wear scar diameter alone is insufficient for characterizing four-ball wear. The comparison of the WPs of all the trial oils shows that the CuO and MoS_2 nanoparticle-enriched lubricants improved by 12.5% and 18.75%, respectively. **Fig. 7** presents the wear data on the cylinder liner that was tested to determine the sliding wear characteristics of the trial oils. The extent of wear was correlated with the effectiveness of the lubricants, with CMPO showing wear higher than that occurring with the use of the nanolubricants. Oil F provided the most satisfactory protection against sliding wear because weight loss decreased by 29% compared with the loss achieved with the blank CMPO. The nanolubricant with the CuO nanoparticles and no surfactant exhibited minimal anti-wear behavior because a reduction of merely 4% was achieved with Oil C. This wear

behavior of the CuO-enriched lubricants may be attributed to the poor dispersibility of CuO in CMPO; by contrast, MoS_2 exhibited excellent dispersibility **(Fig. 4)**. Adding the surfactant in the CuO nanoparticles enabled uniform dispersion and improved wear protection given that weight loss decreased by 20% with Oil E. This result indicates that the synthesized nanolubricants are suitable materials for sliding contact under medium loading conditions. A similar wear reduction at sliding contact was observed by other researchers upon the addition of 1% CuO [15] and 1% MoS_2 with and without surfactants [24]. In terms of sliding conformal contact geometry, wear reduction can be linked to tribofilm formation on interacting surfaces. Such formation is a result of the reaction between a material, additives, and the environment in which lubricated sliding contact is induced [24]. The tested and new cast-iron liner specimens were analyzed by Raman spectroscopy to confirm the formation of tribofilms on the surface of the cylinder liner **(Fig. 11)**.

Table 6. LNSL, ISL and LWI and WP values for oil samples.

Fig.7. Wear of cylinder liner specimen after sliding wear tests.

3.2. SEM and EDX analyses

The worn surfaces of the tested balls were characterized by SEM and EDX spectroscopy. The detailed microscopic views of the wear scars produced under specific ISLs were selected for the characterization **(Fig. 8)**. The role of the nanolubricants in diminishing the wear scar diameters is illustrated in **Figs. 8(a)–8(f)**. The scratched grooves on the wear scar produced with oils A and B are presented in **Figs. 8(a) and 8(b)**, respectively. Smooth surfaces were

observed, and minor pits replaced the scratched grooves **(Figs. 8(c)–8(f))**. The smooth surfaces are related to the nanoparticle precipitation that occurred on the contact surface; the difference between CMPO and the nanolubricants reflects the effectiveness of the nanoparticles. The CuO nanoparticles were non-uniformly distributed on the surface, and agglomerates can be observed in **Fig. 8(c)**. The agglomeration of the CuO nanoparticles is due to low dispersibility in the absence of a surfactant. Accordingly, the addition of the surfactant suppressed the agglomeration of the CuO nanoparticles and reduced wear scar diameter (**Fig. 8(e))**. These phenomena highlight the significance of uniform nanoparticle dispersion for improved wear protection. The wear scar surface of the balls treated with MoS_2 nanoparticle-enriched CMPO was slightly affected by the surfactant addition **(Figs. 8(d) and 8(f))**. For the examined four-ball test geometry and ISL, tribo-sintering of the nanoparticles was observed at large magnifications (**Figs. 8(i)**, **8(j)**, **8(k)**, **and 8(l)** for oils C, D, E, and F, respectively). The tribo-sintering of the nanometer-sized particles as solid lubricants was verified by Kato et al. [33]. The mechanism of material filling by the nanoparticles has also been reported by other researchers [8, 13, 34]. For the extreme pressure test conditions investigated, high temperatures were achieved at non-conformal ball contact under ISL. According to Zhou et al. [35], tribo-sintering initializes as soon as temperature increases to above-room levels for the very fine metal powders in a lubrication system. Under non-conformal contact geometry and extreme loading conditions, therefore, the wear mechanism of tribo-sintering could be observed in the present work. The nanoparticle deposition on the worn surfaces was further confirmed by the EDX analysis. The electron image of the selected wear scar and the related elemental details for the nanolubricants are presented in **Figs. 9** and **10**, respectively. The EDX analysis shows that the CuO and MoS_2 nanoparticles were sintered on the wear scratches, thereby enabling the materials to provide wear protection. **Table 7** lists the elemental weight percentages of the wear scars on the specimens treated with the trial oils. A

high Cu content (i.e., 11.65%) was observed on the scar surface of the specimen treated with Oil C; this concentration can be attributed to the agglomeration of the CuO particles in the absence of a surfactant **(Fig. 8(c))**. Although all the examined nanolubricants exhibited the wear protection mechanism of tribo-sintering in the four-ball tests on resistance to extreme pressure, the CuO-enriched nanolubricants tended to form agglomerates. Such agglomeration, in turn, resulted in lesser wear protection.

Fig. 8. The morphology of the wear scar of CMPO and nanoparticle additives and the distribution of Cu, Mo, S on the rubbed surface: (a) wear scar by Oil A (25x), (b) wear scar by Oil B (25x), (c) wear scar by Oil C (25x), (d) wear scar by Oil D (25x), (e) wear scar by Oil E (25x), (f) wear scar by Oil F (25x), (g) distribution of CMPO (500x), (h) distribution of CMPO+S (500x),(i) distribution of CuO (500x),(j) distribution of MoS_2 (500x) (k) distribution of CuO+S (500x) and (l) distribution of MoS_2+S (500x).

Fig. 9. Micrograph and elemental analysis of Oil E at initial seizure load.

Fig. 10. Micrograph and elemental analysis of Oil F at initial seizure load.

Table 7. Elemental details of worn surfaces at initial seizure load.

3.3. Raman spectroscopy

Tribofilms and near-surface materials govern the tribological behaviors of interacting surfaces. The CuO- and MoS_2-enriched nanolubricants formed tribofilms, thereby facilitating the reduction of sliding wear. When the cylinder liner specimen were lubricated with the nanolubricant samples, tribofilms formed on the surface of the cast-iron cylinder liner during sliding motion against piston ring. Micro-Raman spectroscopy was performed to further investigate protective film formation. The micro-Raman spectra of an untreated cast-iron cylinder surface, a cast-iron liner specimen treated with Oil E, and a cast-iron liner specimen treated with Oil F were obtained **(Fig. 11)**. The monoclinic CuO in nanolubricant F produced three Raman peaks at 293, 343, and 626 cm^{-1} for the treated cast-iron liner specimen **(Fig. 11)**. CuO belongs to the C^6_{2h} with nine zone-center optical phonon modes, out of which only three (A_g+$2B_g$) modes are Raman active [36]. The three Raman peaks can therefore be assigned to the A_g mode at 293 cm^{-1} and to the B_g modes at 343 and 626 cm^{-1} for the active Raman spectra. The Raman peaks produced by the cylinder liner specimen treated with the CuO nanolubricant are closely related to those produced by the CuO nanocrystals discussed in previous research [36, 37]. This similarity confirms the tribofilm formation on the cylinder liner surface; the formation was triggered by the reaction between the treated material and the additives under the provided environment. The micro-Raman spectroscopic results on the MoS_2-based nanolubricants with a surfactant showed intensity peaks at 385, 407, and 642 cm^{-1} **(Fig. 11)**. The acquired spectra for the MoS_2-treated cylinder specimen are similar to the pattern of MoS_2 resonant Raman spectra that occurs under argon ion laser excitation at 532 nm [38]. The resonant Raman peaks result from the oscillation of atoms in the S–Mo–S layer [24, 39]. In the current work, tribofilm formation is confirmed by the fact that the Raman peaks produced by the MoS_2-treated cylinder specimen agree well with the Raman spectra obtained by other researchers [24, 38]. The formation of peaks near 1300 ± 10 cm^{-1} and 1450 ± 10 cm^{-1} was caused by the phase vibration and distortion of the (CH3–) and (–CH2–)

groups, whereas the Raman peaks between 843 and 891 cm^{-1} are related to (H–C=). The bands in the 1064 to 1079 cm^{-1} range are attributed to C=C=C stretching [40]. The investigation of the cylinder liner surface shows that the wear protection mechanism of tribofilm formation resulted for reciprocating conformal contact geometry. Although all the investigated nanolubricants enriched with nanoCuO and nanoMoS_2 showed tribofilm formation, the MoS_2-enriched CPMO exhibited the lowest cylinder liner wear (**Fig. 7)**. This tendency of MoS_2 may be related to the aligned tribofilm formation that is due to the uniform dispersion of MoS_2 in CMPO.

Fig. 11. Raman spectra of cast iron cylinder liners tested with Oil E and Oil F.

4. Conclusion

The effects of CuO and MoS_2 on the AW/EP properties of CMPO were investigated. The conclusions drawn from the results are summarized as follows:

- CuO and MoS_2 nanoparticles were effective additives for incorporation into CMPO; they enhanced AW/EP properties by 1.5 times.
- MoS_2-enriched nanolubricants enabled more uniform dispersion and AW/EP characteristics that are superior to that achieved with CuO-dispersed oils, as indicated by the tribological investigation of four ball and piston ring on cylinder liner test geometries.
- Contact geometry, dynamics, and testing conditions govern the wear protection mechanisms irrespective of type of nanolubricant used in this study. For considered nanolubricants, tribo-sintering was observed under non-conformal contact geometry in the

four-ball EP test whereas tribofilms formation was reported for piston ring on cylinder liner wear tests.

- The addition of oleic acid as surfactant not only aided nanoparticle suspension but also reduced wear, as determined in the dispersion analysis and four-ball standard test respectively.

Acknowledgements

The authors would like to thank the University of Malaya, which made this study possible through the High Impact Research Chancellory Grant, Project title: ‘‘Development of Alternative and Renewable Energy Carrier’’ Grant Number: UM.C/HIR/MOHE/ENG/60 and UMRG Grant RP016-2012A.

References

[1] Kodali DR. High performance ester lubricants from natural oils. Industrial lubrication and tribology. 2002;54:165-70.
[2] Arumugam S, Sriram G. Synthesis and characterisation of rapeseed oil bio-lubricant–its effect on wear and frictional behaviour of piston ring–cylinder liner combination. Proceedings of the Institution of Mechanical Engineers, Part J: Journal of Engineering Tribology. 2012;227:3-15.
[3] Zulkifli NWM, Kalam MA, Masjuki HH, Shahabuddin M, Yunus R. Wear prevention characteristics of a palm oil-based TMP (trimethylolpropane) ester as an engine lubricant. Energy. 2013;54:167-73.
[4] Fox NJ, Stachowiak GW. Vegetable oil-based lubricants—A review of oxidation. Tribology International. 2007;40:1035-46.
[5] Shahabuddin M, Masjuki HH, Kalam MA. Experimental Investigation into Tribological Characteristics of Bio-Lubricant Formulated from Jatropha Oil. Procedia Engineering. 2013;56:597-606.
[6] Masjuki H, Maleque M. Investigation of the anti-wear characteristics of palm oil methyl ester using a four-ball tribometer test. Wear. 1997;206:179-86.
[7] Lee K, Hwang Y, Cheong S, Choi Y, Kwon L, Lee J, et al. Understanding the Role of Nanoparticles in Nano-oil Lubrication. Tribology Letters. 2009;35:127-31.
[8] Choi Y, Lee C, Hwang Y, Park M, Lee J, Choi C, et al. Tribological behavior of copper nanoparticles as additives in oil. Current Applied Physics. 2009;9:e124-e7.
[9] Liu G, Li X, Lu N, Fan R. Enhancing AW/EP property of lubricant oil by adding nano Al/Sn particles. Tribology Letters. 2005;18:85-90.

[10] Wu Y, Tsui W, Liu T. Experimental analysis of tribological properties of lubricating oils with nanoparticle additives. Wear. 2007;262:819-25.
[11] Zhou J, Wu Z, Zhang Z, Liu W, Xue Q. Tribological behavior and lubricating mechanism of Cu nanoparticles in oil. Tribology Letters. 2000;8:213-8.
[12] Yu H-l, Xu Y, Shi P-j, Xu B-s, Wang X-l, Liu Q. Tribological properties and lubricating mechanisms of Cu nanoparticles in lubricant. Transactions of Nonferrous Metals Society of China. 2008;18:636-41.
[13] Yu HL, Xu Y, Shi PJ, Xu BS, Wang XL, Liu Q, et al. Characterization and nano-mechanical properties of tribofilms using Cu nanoparticles as additives. Surface and Coatings Technology. 2008;203:28-34.
[14] Alves SM, Barros BS, Trajano MF, Ribeiro KSB, Moura E. Tribological behavior of vegetable oil-based lubricants with nanoparticles of oxides in boundary lubrication conditions. Tribology International. 2013;65:28-36.
[15] Hernández Battez A, González R, Viesca JL, Fernández JE, Díaz Fernández JM, Machado A, et al. CuO, ZrO_2 and ZnO nanoparticles as antiwear additive in oil lubricants. Wear. 2008;265:422-8.
[16] Arumugam S, Sriram G. Synthesis and characterization of rapeseed oil bio-lubricant dispersed with nano copper oxide: Its effect on wear and frictional behavior of piston ring–cylinder liner combination. Proceedings of the Institution of Mechanical Engineers, Part J: Journal of Engineering Tribology. 2014;228:1308-18.
[17] Hernández Battez A, González R, Felgueroso D, Fernández JE, del Rocío Fernández M, García MA, et al. Wear prevention behaviour of nanoparticle suspension under extreme pressure conditions. Wear. 2007;263:1568-74.
[18] Asrul M, Zulkifli NWM, Masjuki HH, Kalam MA. Tribological Properties and Lubricant Mechanism of Nanoparticle in Engine Oil. Procedia Engineering. 2013;68:320-5.
[19] Thottackkad MV, Perikinalil RK, Kumarapillai PN. Experimental evaluation on the tribological properties of coconut oil by the addition of CuO nanoparticles. International Journal of Precision Engineering and Manufacturing. 2012;13:111-6.
[20] Hernandez Battez A, Fernandez Rico JE, Navas Arias A, Viesca Rodriguez JL, Chou Rodriguez R, Diaz Fernandez JM. The tribological behaviour of ZnO nanoparticles as an additive to PAO6. Wear. 2006;261:256-63.
[21] Ma S, Zheng S, Cao D, Guo H. Anti-wear and friction performance of ZrO2 nanoparticles as lubricant additive. Particuology. 2010;8:468-72.
[22] Chen J. Tribological properties of polytetrafluoroethylene, nano-titanium dioxide, and nano-silicon dioxide as additives in mixed oil-based titanium complex grease. Tribology letters. 2010;38:217-24.
[23] Luo T, Wei X, Huang X, Huang L, Yang F. Tribological properties of Al_2O_3 nanoparticles as lubricating oil additives. Ceramics International. 2014;40:7143-9.
[24] Demas NG, Timofeeva EV, Routbort JL, Fenske GR. Tribological effects of BN and MoS_2 nanoparticles added to polyalphaolefin oil in piston skirt/cylinder liner tests. Tribology Letters. 2012;47:91-102.
[25] Yadgarov L, Petrone V, Rosentsveig R, Feldman Y, Tenne R, Senatore A. Tribological studies of rhenium doped fullerene-like MoS_2 nanoparticles in boundary, mixed and elasto-hydrodynamic lubrication conditions. Wear. 2013;297:1103-10.
[26] Rabaso P, Ville F, Dassenoy F, Diaby M, Afanasiev P, Cavoret J, et al. Boundary lubrication: Influence of the size and structure of inorganic fullerene-like MoS_2 nanoparticles on friction and wear reduction. Wear. 2014;320:161-78.
[27] Kalin M, Kogovšek J, Remškar M. Mechanisms and improvements in the friction and wear behavior using MoS_2 nanotubes as potential oil additives. Wear. 2012;280–281:36-45.
[28] Nallasamy P, Saravanakumar N, Nagendran S, Suriya E, Yashwant D. Tribological investigations on MoS_2-based nanolubricant for machine tool slideways. Proceedings of the Institution of Mechanical Engineers, Part J: Journal of Engineering Tribology. 2014;doi: 10.1177/1350650114556394.

[29] Gullac B, Akalin O. Frictional characteristics of IF-WS_2 nanoparticles in simulated engine conditions. Tribology Transactions. 2010;53:939-47.
[30] Rapoport L, Leshchinsky V, Lapsker I, Volovik Y, Nepomnyashchy O, Lvovsky M, et al. Tribological properties of WS_2 nanoparticles under mixed lubrication. Wear. 2003;255:785-93.
[31] Arumugam S, Sriram G, Ellappan R. Bio-lubricant-biodiesel combination of rapeseed oil: An experimental investigation on engine oil tribology, performance, and emissions of variable compression engine. Energy. 2014;72:618-27.
[32] Menezes P, Ingole SP, Nosonovsky M, Kailas SV, Lovell MR. Tribology for Scientists and Engineers: Springer Science+ Business Media New York; 2013.
[33] Kato H, Komai K. Tribofilm formation and mild wear by tribo-sintering of nanometer-sized oxide particles on rubbing steel surfaces. Wear. 2007;262:36-41.
[34] Padgurskas J, Rukuiza R, Prosyčevas I, Kreivaitis R. Tribological properties of lubricant additives of Fe, Cu and Co nanoparticles. Tribology International. 2013;60:224-32.
[35] Zhou Y-H, Harmelin M, Bigot J. Sintering behaviour of ultra-fine Fe, Ni and Fe-25wt% Ni powders. Scripta metallurgica. 1989;23:1391-6.
[36] Xu J, Ji W, Shen Z, Li W, Tang S, Ye X, et al. Raman spectra of CuO nanocrystals. Journal of Raman spectroscopy. 1999;30:413-5.
[37] Zhu J, Bi H, Wang Y, Wang X, Yang X, Lu L. CuO nanocrystals with controllable shapes grown from solution without any surfactants. Materials Chemistry and Physics. 2008;109:34-8.
[38] Wang Z, Chen T, Chen W, Chang K, Ma L, Huang G, et al. CTAB-assisted synthesis of single-layer MoS_2–graphene composites as anode materials of Li-ion batteries. Journal of Materials Chemistry A. 2013;1:2202-10.
[39] Wieting TJ, Verble JL. Infrared and Raman Studies of Long-Wavelength Optical Phonons in Hexagonal MoS_2. Physical Review B. 1971;3:4286-92.
[40] Mayo DW, Miller FA, Hannah RW, Wesley R. Course notes on the interpretation of infrared and Raman spectra: Wiley Online Library; 2004.

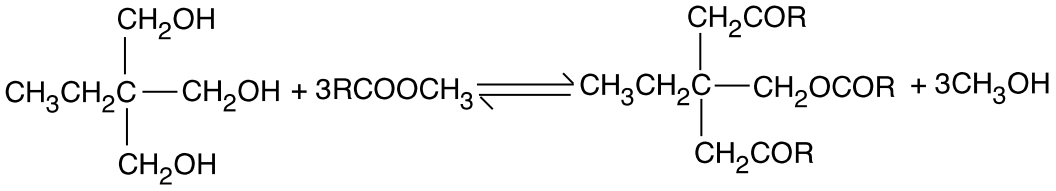

TMP POME TMP ester (CMPO) Methanol

R=alkyl group C_6-C_{20}

Fig.1. Overall reaction for synthesis of CMPO

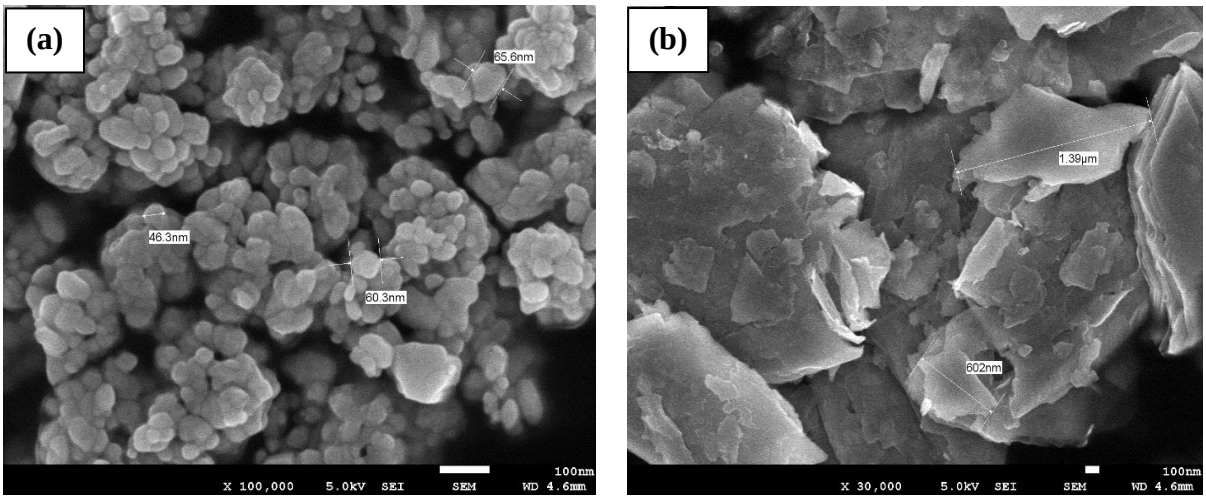

Fig.2. SEM micrographs of (a) CuO nanoparticles (b) MoS_2 nanoparticles.

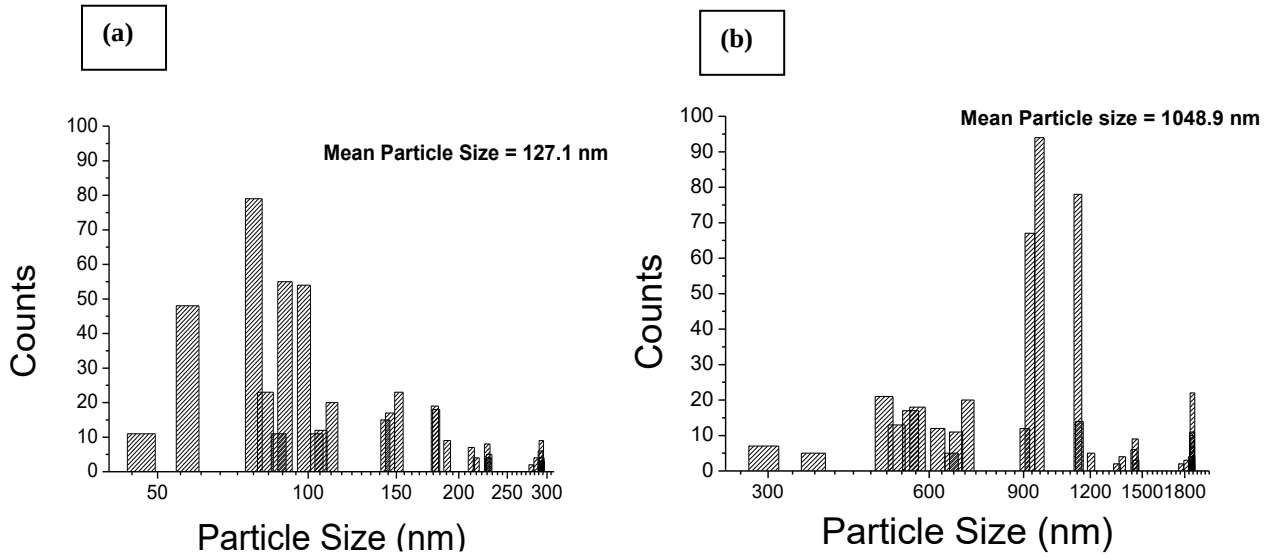

Fig.3. Lognormal size distribution with mean particle size (a) nanoCuO (b) nanoMoS_2

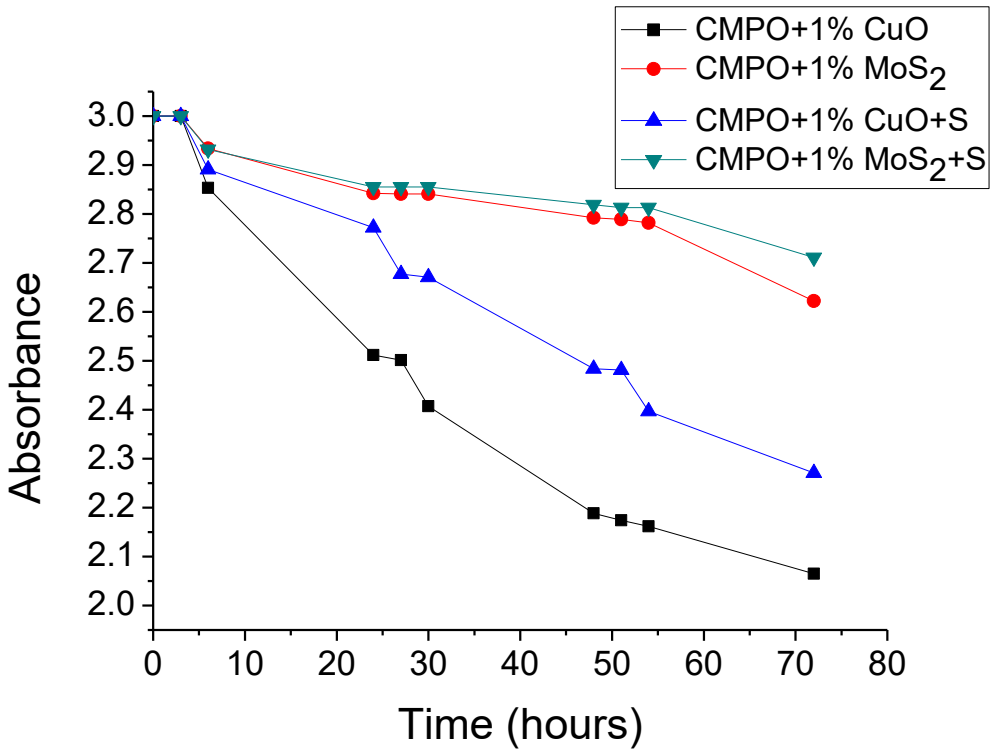

Fig. 4. The optical absorbance spectrum of nanolubricant samples over time.

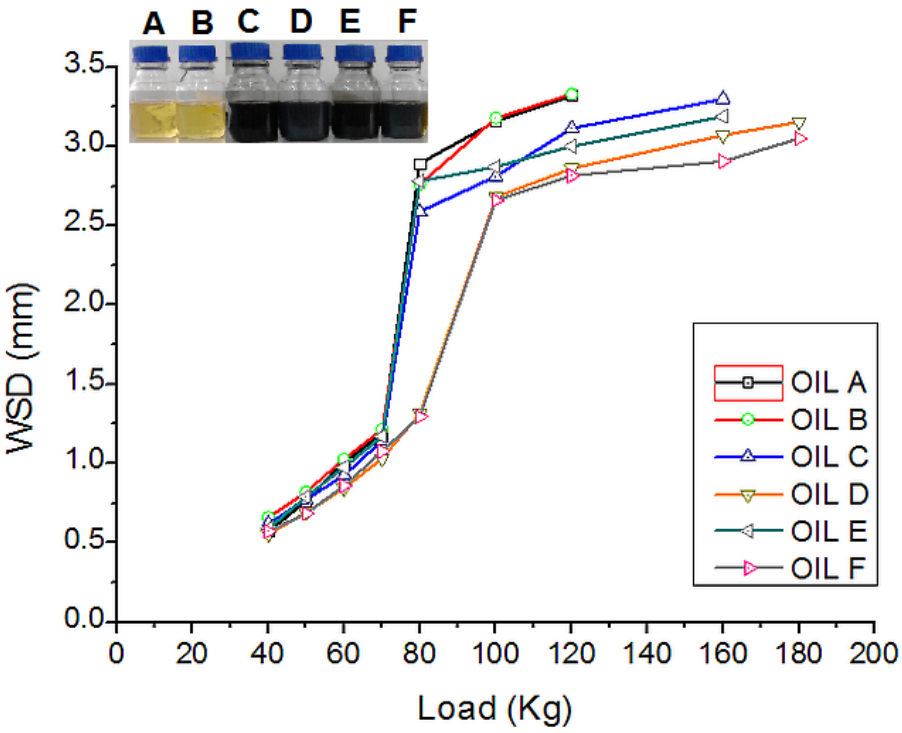

Fig. 5. Load vs. wear scar diameter (WSD) of CMPO+ nanoparticles suspensions.

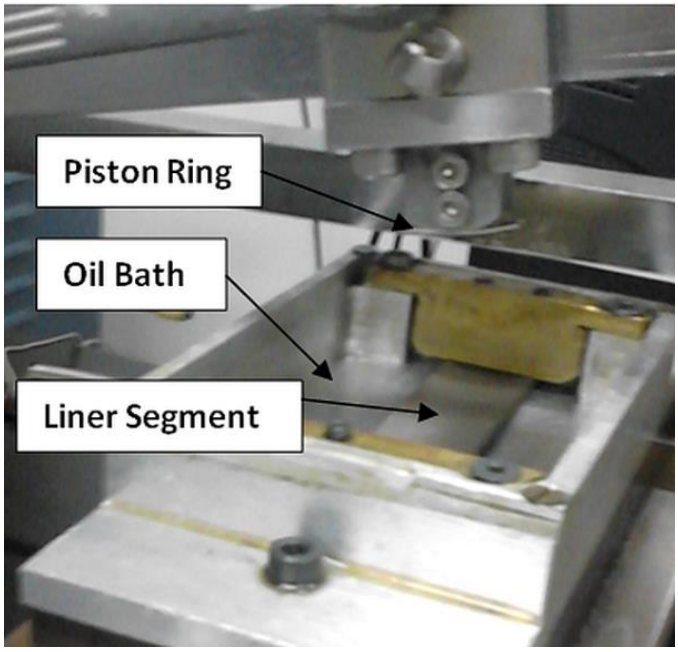

Fig. 6. Experimental setup for piston ring on liner wear testing.

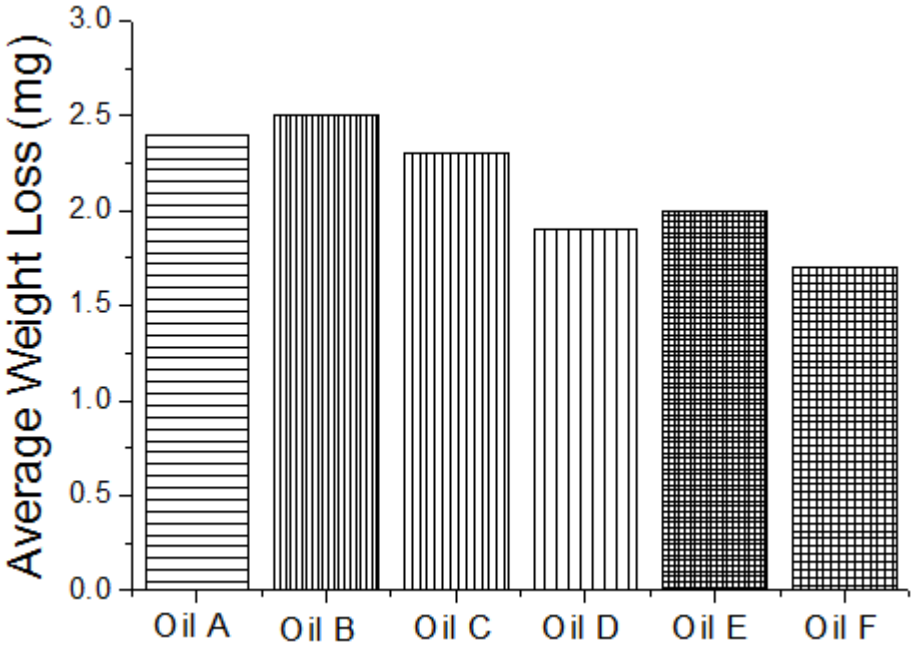

SD	0.1414	0.0707	0.2828	0.1414	0.0707	0.1414

Fig.7. Wear of cylinder liner specimen after sliding wear tests.

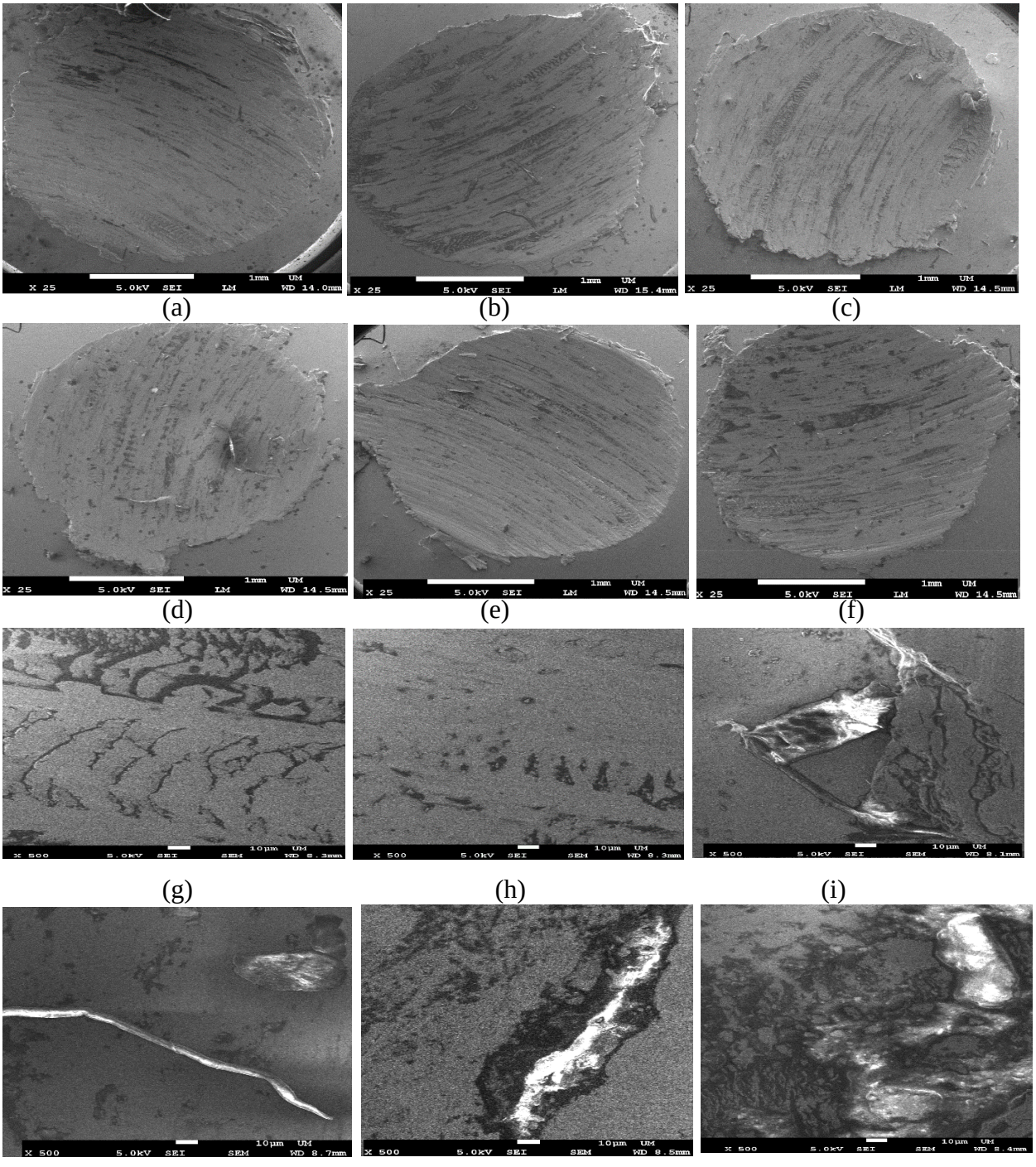

Fig. 8. The morphology of the wear scar of CMPO and nanoparticle additives and the distribution of Cu, Mo, S on the rubbed surface: (a) wear scar by Oil A (25x), (b) wear scar by Oil B (25x), (c) wear scar by Oil C (25x), (d) wear scar by Oil D (25x), (e) wear scar by Oil E (25x), (f) wear scar by Oil F (25x), (g) distribution of CMPO (500x), (h) distribution of

CMPO+S (500x),(i) distribution of CuO (500x),(j) distribution of MoS_2 (500x) (k) distribution of CuO+S (500x) and (l) distribution of MoS_2+S (500x).

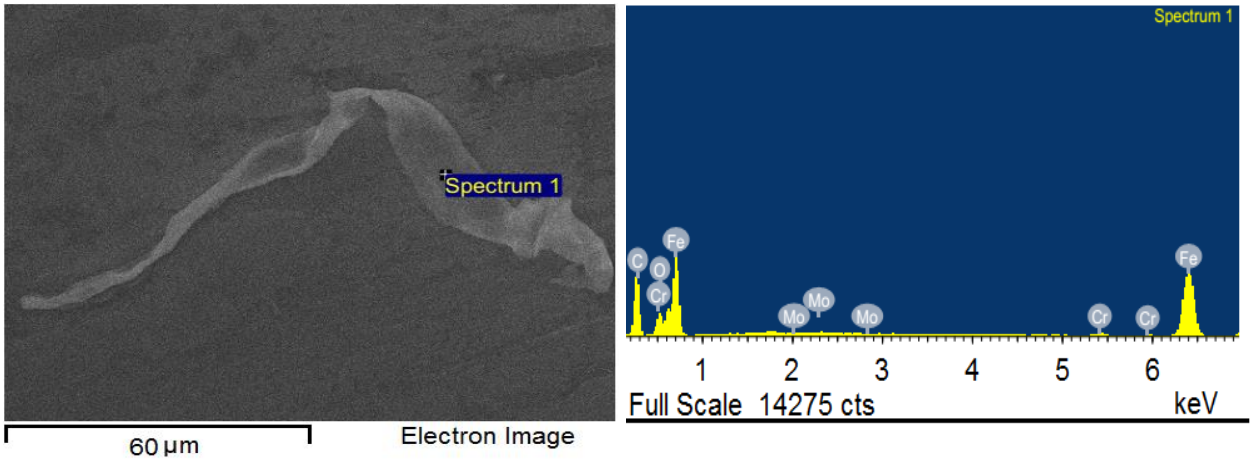

Fig.9. Micrograph and elemental analysis of Oil E at initial seizure load.

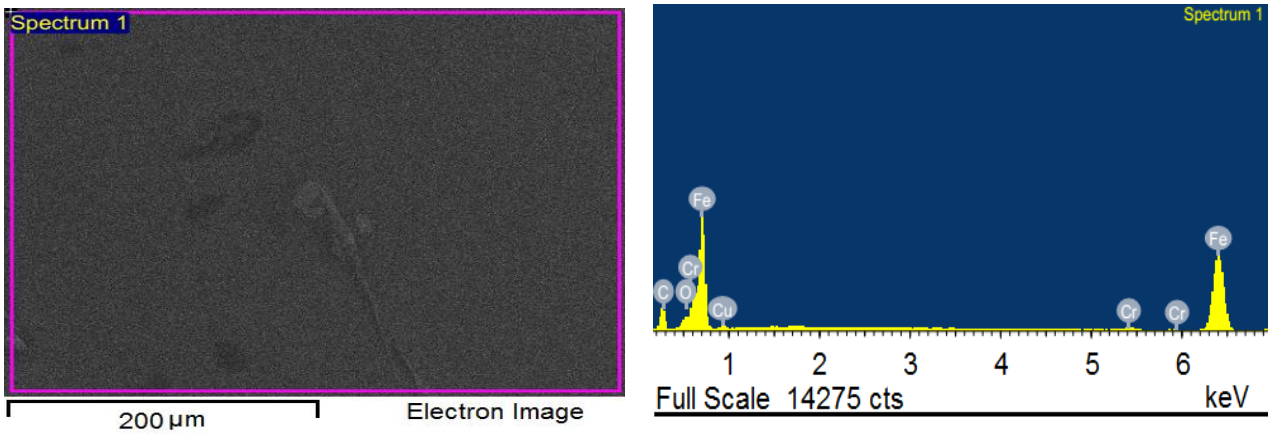

Fig.10. Micrograph and elemental analysis of Oil F at initial seizure load.

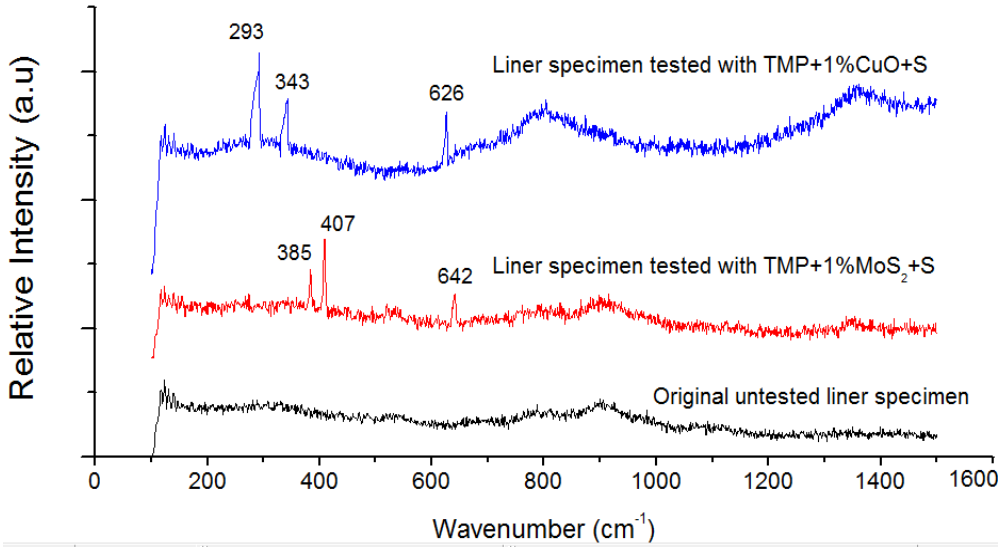

Fig.11. Raman spectra of cast iron cylinder liners tested with Oil E and Oil F.

Table 1. Material properties of nanoparticles

Materials	Properties						
Nanoparticles	Crystal System	Purity (%)	Morphology	Relative Density (g/cm^3)	Molecular Weight (g/mol)	Melting Point (^0C)	Hardness (Moh)
CuO	Monoclinic	99.99	Nearly spherical	6.32	79.55	1336	3.5
MoS_2	Hexagonal	99	Non-spherical	5.06	160.07	2375	1.0

Table 2. Physicochemical properties of lubricant samples

Sample	Properties					
	Viscosity ASTM D7042		VI	Density	TAN ASTM D664	TBN ASTM D2896
	40 ºC (cSt)	100 ºC (cSt)		15 ºC (g/cm^3)	(mgKOH/g)	
CMPO	40.031	9.155	221	0.9011	0.44	0.37
CMPO + S	39.273	9.065	223	0.8983	0.53	0.48
CMPO + 1% CuO	40.252	9.181	220	0.9144	0.47	0.41
CMPO+1% MoS_2	40.959	9.297	220	0.9079	0.45	0.40
CMPO+1% CuO+S	40.171	9.184	221	0.9067	0.52	0.49
CMPO+1% MoS_2+S	40.091	9.163	221	0.9022	0.51	0.49

Table 3. Test conditions for four-ball tests

Condition	Value
Test Temperature (^{o}C)	25±5
Test Duration (sec)	10
Spindle Speed (rpm)	1770 ± 30
Load (Kg)	Varies, 10-sec/stage
Ball Material	AISI 52100
Ball Diameter (mm)	12.7
Ball Hardness (HRC)	64-66

Table 4. Wear scar diameter of test balls

Load/Kg Oil sample		Average wear scar diameter/mm								
		40	50	60	70	80	100	120	160	180
CMPO (Oil A)	Min	0.58	0.76	0.98	1.15	2.89	3.18	3.34		
	Mean	0.62	0.81	1.05	1.24	2.94	3.21	3.37		
	Max	0.66	0.87	1.13	1.33	2.98	3.24	3.42		
	SD	0.052	0.07	0.098	0.108	0.052	0.048	0.056		
CMPO+1%S	Min	0.58	0.80	0.94	1.12	2.54	3.06	3.31		
(Oil B)	Mean	0.66	0.82	1.02	1.21	2.76	3.18	3.33		
	Max	0.74	0.84	1.11	1.31	2.98	3.30	3.40		
	SD	0.109	0.028	0.101	0.13	0.26	0.147	0.071		
CMPO+1%CuO	Min	0.55	0.71	0.87	1.05	2.47	2.78	2.96	3.26	
(Oil C)	Mean	0.62	0.77	0.92	1.14	2.59	2.81	3.11	3.30	
	Max	0.69	0.84	0.98	1.24	2.71	2.84	3.27	3.34	
	SD	0.098	0.084	0.071	0.124	0.147	0.050	0.194	0.058	
CMPO+1%MoS_2	Min	0.48	0.63	0.81	0.93	1.11	2.64	2.83	3.04	3.13
(Oil D)	Mean	0.55	0.69	0.84	1.03	1.31	2.68	2.86	3.07	3.15
	Max	0.63	0.75	0.88	1.13	1.51	2.72	2.89	3.10	3.18
	SD	0.093	0.090	0.043	0.132	0.235	0.075	0.054	0.058	0.071
CMPO+1%CuO+	Min	0.54	0.74	0.81	1.08	2.64	2.86	2.98	3.14	
1%S (Oil E)	Mean	0.59	0.79	0.97	1.17	2.78	2.87	3.00	3.16	
	Max	0.64	0.84	1.14	1.26	2.92	2.88	3.02	3.19	
	SD	0.096	0.069	0.207	0.106	0.165	0.018	0.026	0.037	
CMPO+1%	Min	0.51	0.61	0.81	1.02	1.18	2.64	2.76	2.88	3.04
MoS_2+1%S (Oil F)	Mean	0.57	0.68	0.86	1.07	1.29	2.66	2.81	2.90	3.05
	Max	0.63	0.76	0.91	1.13	1.41	2.68	2.87	2.93	3.07
	SD	0.090	0.103	0.095	0.083	0.168	0.052	0.091	0.059	0.041

The load values corresponding to cells with grey background show the LNSL values of relevant lubricant samples.

Table 5. Test parameters with values for ring on cylinder test

Normal load	160 N
Temperature	70 ^{0}C
Stroke	84 mm
Contact width	25.4 mm
Speed	240 rpm
Lubricant feed rate	5 mL/hr
Test duration	6 hrs

Table 6. LNSL, ISL and LWI and WP values for oil samples.

	Oil A	Oil B	Oil C	Oil D	Oil E	Oil F
LNSL/Kg	70	70	70	80	70	80
ISL/Kg	80	80	80	100	80	100
LWI/Kg	19.26	18.09	19.26	21.71	20.24	20.95
WP/Kg	160	160	180	190	180	190

Table 7. Elemental details of worn surfaces at initial seizure load.

Element	Oil A	Oil B	Oil C	Oil D	Oil E	Oil F
	wt%	wt%	wt%	wt%	wt%	wt%
C K	17.1	17.05	19.17	58.86	16.94	32.94
O K	3.18	3.18	3.84	11.33	2.47	6.63
Cr K	1.39	1.39	1.19	0.53	1.17	1.07
Fe K	78.02	78.07	64.14	28.37	76.17	58.79
Si K	0.31	0.31	0	0	0	0
Cu L	0	0	11.65	0	3.25	0
Mo L	0	0	0	0.74	0	0.57
S K	0	0	0	0.17	0	0